Multi-Beam Strategies for the Optimization of the Selective Laser Melting Process

T. Heeling, L. Zimmermann, K. Wegener

Institute of Machine Tools and Manufacturing, ETH Zurich, 8092 Zurich, Switzerland

Abstract

The additive manufacturing of metal parts is of increasing importance for various industry sectors, but processes like selective laser melting are still lacking of robustness especially in the case of hard to process materials. The local adjustment of temperature fields around the melt pool seems promising to decrease melt pool and stress related defects because the boundary conditions can be tailored to positively influence the melt pool dynamics and lifetime as well as the temperature gradients which are the main reason for distortion and cracking. Therefore a selective laser melting laboratory machine was built up which features two independent lasers and beam deflection units which are adapted to synchronization. To discuss the usability of different synchronized multi-beam strategies for further process improvement, computational and experimental evaluations are used to investigate the strategies' influences on the process dynamics of the selective laser melting process.

Keywords: Selective Laser Melting, Multi-Beam Strategies, 316L

Introduction

Additive manufacturing processes enable the production of parts of nearly unlimited complexity without the need for specific tools. The selective laser melting (SLM) process uses laser sources to irradiate and melt powder particles which were previously distributed onto a building plate in a layer wise manner. Therefore the part is built up step by step until the final height is reached. But due to the repetitive melting and consolidating of material the parts are strongly influenced by residual stresses, distortion and cracking as well as not stress related effects like porosity and a high surface roughness. Especially the stress related defects are limiting the range of materials which can be processed by SLM. To reduce the residual stresses in the manufactured parts, the parts are often heat treated before being cut from the building plate. But this only allows a reduction of distortion after the build is done and therefore cannot increase the range of materials because it cannot influence the process itself. That is why an online manipulation of the stress generation needs to be established. Since the stresses mainly originate in the high temperature gradients [1], often the building plate is heated to homogenize the temperature field and to reduce the cooling speeds [1, 2, 3]. But this effect loses its usability with increasing part heights because the distance to the heating source is increasing. Furthermore the heating temperatures are often limited to about 200°C and all parts on the building plate are effected at once. Another influencing factor for residual stresses in SLM parts is the scanning strategy. Kruth et al. [2] as well as Shiomi et al. [4] show that a reduction of residual stresses is possible by applying checkerboard / island strategies or strategies for pre- or post-heating of the layers with the melting beam. Using the melting beam for pre- or post-heating reduces the building rate significantly so that a second beam should be considered to apply heating strategies. In addition a second beam enables many other strategies for directly influencing the vicinity of the melt pool and thereby influencing the melt pool dynamics, the temperature field and gradients as well as the cooling rates and thereby the consolidation of the material.

Multi-Beam Strategies

       In selective laser melting multi-beam strategies are usually known to be used to work parallel on multiple parts to increase productivity [5]. Just few publications describe the use of a second laser beam to influence the vicinity of the melt pool in the SLM process, but similar strategies are known from bifocal-hybrid-welding [6] or electron beam welding/melting in which the electron beam can be deflected with very high speeds so that multiple spots can be maintained [7, 8, 9]. In these welding applications a reduction of cracking and distortion could successfully be achieved [6, 8, 9]. In SLM Abe et al. [10] were the first to introduce a multi-beam approach, using a widened spot of a CO_2-laser that follows the melting beam. By reducing the cooling speeds an increase in hardness and strength was achieved but publications to follow up the promising results seem not to be available. Wilkes et al. [11] used a second static but high power beam to irradiate the whole building plate at once and thereby homogenizing the temperature field on an elevated level as high as 1600 °C to enable the processing of ceramics.

       But the overall heating of the building plate to very high temperatures increases the challenges of machine design significantly and does not allow a specific adjustment of the processing strategies for different parts in a single build. That is why a local adjustment of the temperature field by a second laser beam which can be used independently, fully or layer wise synchronized to the first laser beam seems more promising. Therefore the presented strategies follow up on the experiments of Abe et al. [10] using a different set-up and aiming for a reduction of distortion rather than an increase in strength. The strategies are numerically investigated and experimentally validated on a laboratory machine.

Set-up

The laboratory machine features two independent lasers and beam deflection units with a wide scan field overlap which are adapted to synchronization. The laser units deliver beams of 1070 nm wavelength with powers up to 200 W each that are focused to a focal spot diameter of about 90 μm. The scan fields' overlap is 160 mm wide so that the complete building plate of 100 mm diameter can be irradiated with both beams at once. The path planning is done using a self-developed matlab based CAD/CAM tool to generate the paths of different synchronized strategies.

       To guarantee a heat input as defined in the scanning strategies a calibration of the scan field is necessary prior to every building process. Therefore a plate is leveled to the chosen focal plane and covered with crosses of both laser sources. The calibration crosses of the second beam are rotated by 45° so that the offset of the crosses' center points can be measured and be used to generate a correction field covering the building plate. The calibration procedure is illustrated in figure 1. The calibration is detailed to remaining errors smaller than a quarter beam diameter in both coordinate directions prior to the building process. A slight shift of the offsets might occur during the building process due to an overall warming of the building chamber.
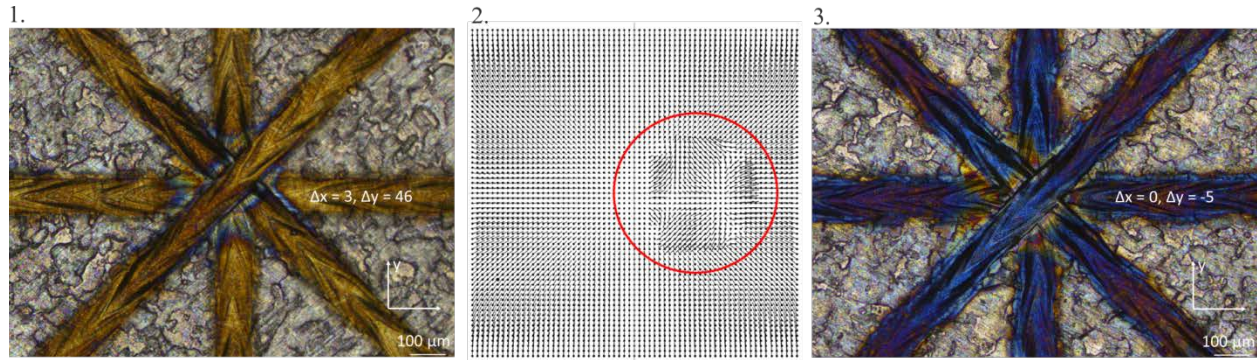
Figure 1: Calibration procedure. 1. Measuring offsets of crossing points distributed over the building plate. 2. Changing the calibration file of scan head 2 to match the scan field of scan head 1. 100 times amplification is shown for the calibration of the building plate area. 3. Measuring offsets after calibration to ensure the necessary accuracy

Elaborated Multi-Beam Strategies

Besides building parts only with one laser beam two scanning strategies using both beams have been developed. One strategy is using both laser beams with a defined offset in scanning direction. In this case the second laser beam follows the first one and therefore irradiates the already molten material aiming to reduce cooling rates and to homogenize the temperature field in the vicinity of the melt pool but to still reach the necessary remelted depth. To allow a defined offset along the part a synchronized motion of all four galvo axes is established. This strategy is later on referred to as *offset strategy*. The second strategy aims for an even better homogenization of the whole part's temperature field on a higher temperature level. Therefore the second beam is used to irradiate the part multiple times using very fast scan speeds while the first beam melts the material as usual so that a layer wise synchronization of the beams is used. This strategy is referred to as *heating strategy* in following sections
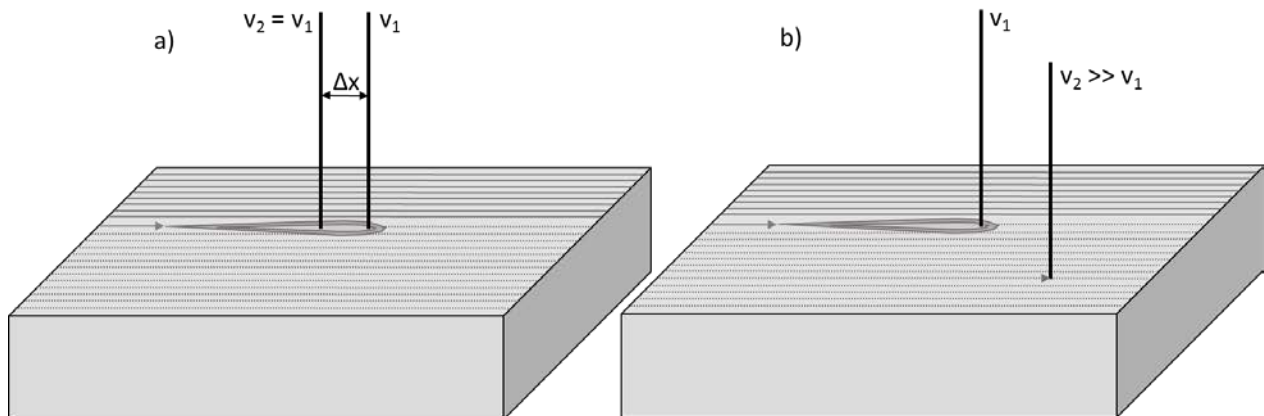

Figure 2: a) Offset strategy: Using two beams in a defined offset at the same speed. b) Heating strategy: Using a melting beam of scan speed v_1 and a heating beam of v_2 which is much faster and irradiates the layer multiple times while beam 1 melts the tracks

Simulation

Numerical Modeling

The numerical model covers the thermodynamics and fluid dynamics on the melt pool level using a weak coupling of the temperature field and fluid flow calculation. It features various physical effects for a detailed representation of the melt pool and its vicinity. In particular the effects of thermal conduction, convection and radiation, melting/freezing and evaporation as well as heat exchange due to melt pool convection are covered in the temperature field calculation using an explicit finite differencing scheme. The fluid flow calculation furthermore covers the effects of buoyancy and capillary forces, the Marangoni effect as well as the recoil pressure as driving forces for the melt flow by elaborating a combined level set volume of fluid method as proposed by Son [12] and Son & Hur [13]. For a detailed representation of the laser energy absorption in the powder bed, solid material and melt pool the model proposed by Gusarov et al. [14] is used and numerically improved by calculating the absorption related parameters element-stack wise so that a lateral differentiation of absorption characteristics can be realized on the scale of a single element size. For the simulation a multi-track problem is assumed in which the laser path is situated next to an idealized solidified track. Furthermore the powder bed is modeled as a homogeneous powder bed that can consolidate due to the melt pool dynamics as illustrated in figure 3.
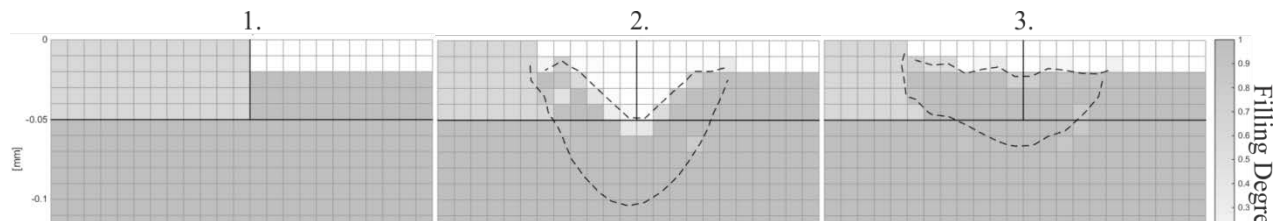

Figure 3: Illustration of a simulated cross section at different time steps. The dashed line represents the melt pool boundary. 1. Initial state of previous layer (bottom), powder (left) and previous track (right). 2. Melt pool geometry at the moment of its deepest state. 3. Geometry of solidifying melt pool

The numerical model was previously validated using cubic probes of 316L processed by a single beam. The relative error in melt pool width and depth was measured to be smaller than 10%.

Material Data

Stainless steel 316L is used in the presented multi-beam experiments. The material is easy to process with SLM and is therefore suitable for a first proof of concept. Furthermore comprehensive material data is provided by the IAEA [15] so that a detailed simulation of the material is possible. The temperature dependent material data which is used for the simulation is listed in table 1. Temperature dependent values are interpolated in between the listed temperature ranges.

Table 1: Material data of stainless steel 316L used for simulation [15, 16]

Parameter	25 °C	1400 °C	1450 °C	2800 °C	constant
Specific Heat Capacity [J/kg K]	450	700	707	900	
Thermal Conductivity [W/m K]	13.30	33.78	18.10	22.20	

Surface Tension [N/m]	1.76	0.41		
Dynamic Viscosity [Pa s]	0.0059	0.0014		
Heat of Fusion [J/kg]			270000	
Heat of Evaporation [J/kg]			7450000	
Hemispherical Reflectivity			0.64	

<u>Influence on the Temperature Field and Melt Pool Dynamics</u>

      The simulation of essential parts of both strategies should support the understanding and increase the definition of processing parameters. In the following the dynamics are exemplarily discussed for a scan speed of 1000 mm/s for the offset strategies with a power ratio of 150 W beam one and 50 W for beam two. The simulations show that the size of the offset is of crucial importance for the melt pool dynamics. Figure 4 shows the simulated dimensions of remolten material.
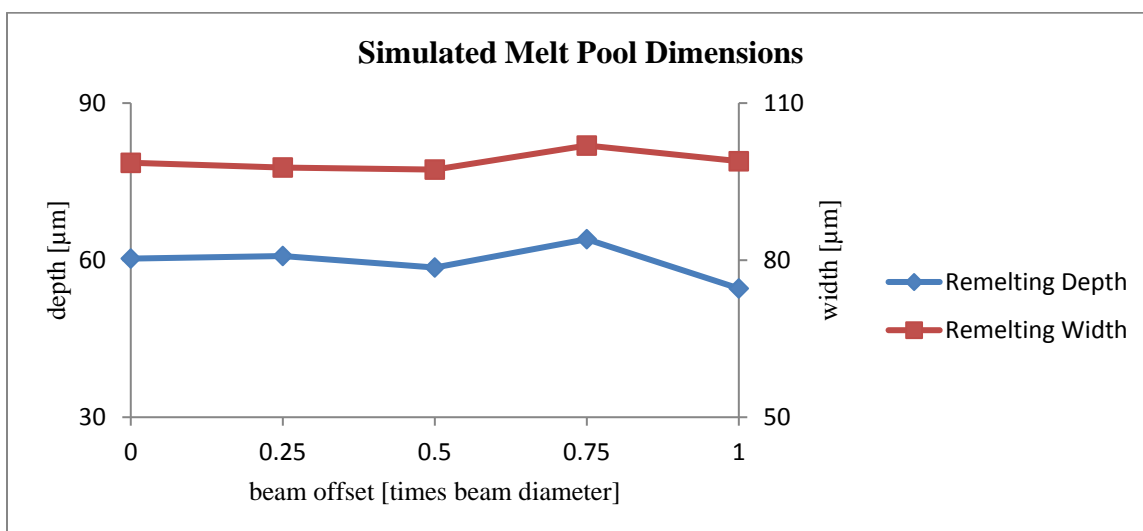

Figure 4: Simulated melt pool dimensions of a track with a scan speed of 1000 mm/s and an overall power of 200 W. For beam offsets the overall power is split into 150 W for beam one and 50 W for beam two.

      The simulation results show a significant dent of remelted width and depth for a beam offset of a half beam diameter while both are larger at a smaller beam offset of a quarter beam diameter as well as at larger offsets of three quarters and a full beam diameter. Therefore a drop in density can be assumed for a beam offset of half a beam diameter since insufficient remelted depth and width are the main reason for porosity. Taking a deeper look in the melt pool dynamics it can be seen that the interaction of the areas in which evaporation takes places due to the irradiation of the beams is responsible for the differences in melt pool dimensions. For an offset of half a beam diameter the second beam irradiates the melt pool front and is supporting evaporation on the front flank which leads to melt pool flows slightly directed to the scanning direction like in the case of no beam offset. But in the case of an offset of half a beam diameter the second beam leads to another evaporation area located directly behind the front flank limiting the backward vortex of the first evaporation area. This leads to a worse distribution of heat and therefore less remelted depth. But in case of an offset of three quarters of a beam diameter the second laser heats the melt even further behind the front flank of the melt pool right where evaporation is already taking place. This leads to a widening of this area so that the downward flows are amplified and a depth greater than the one of a single beam with the same overall

power can be achieved. For higher offsets depth and width of the melt pool continuously decrease. The described differences are plotted figure 5 as the front part of a longitudinal section.
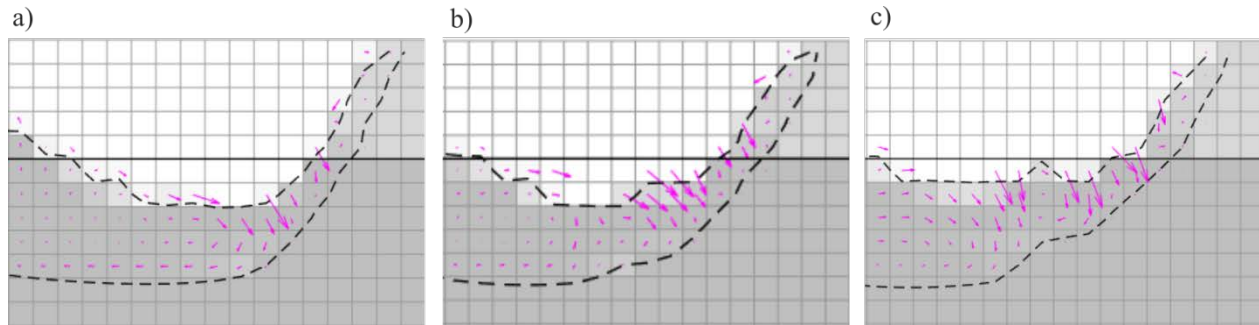

Figure 5: Simulated melt pool fronts in a longitudinal section at 1000 mm/s and different beam offsets. Dashed line represents the melt pool boundary, arrows indicate the melt flow directions and speeds on a relative scale. a) Reference using a single beam at 200 W. b) Beam offset of half a beam diameter. c) Beam offset of three quarters of a beam diameter.

Considering the heating strategy a parameter set is necessary in which the heating beam should not evaporate the material to reduce the chance for spattering. Simulations of single tracks show that a minimum scan speed of 3000 mm/s for the heating laser is necessary to stay below the evaporation temperature at a heating power of 50 W. But considering a continuous heating of the powder and solid material the temperature might as well increase to evaporation temperature using this parameter set.

Furthermore the numerical code can be used to estimate possible benefits of the strategies regarding the residual stresses and distortion. Since no tensile calculations are included the temperature gradients might be used as an indicator. Therefore the maximum temperature gradients on the boundary of melt to solidified material were calculated. The simulations show that the maximum temperature gradient drops with increasing beam offsets by up to 25% at a beam offset of a full beam diameter using a scan speed of 1000 mm/s. These promising results are being validated in the following parts.

Experimental

The experiment is split into two parts: density and distortion. In a first step appropriate process parameters need to be validated to produce high density parts and to separate usable parameter sets from those which are of no use for a possible part production. Therefore 15 cubes of a size of 10x10x10 mm^3 are produced to test different parameter settings. Investigated parameter sets differ in scan speed, power of laser beam 1 and 2 and the offset in scan direction. Based on the presented simulation as well as experience from earlier experiments with only one laser beam the scan speed range is chosen to be between 850 and 1150mm/s. For each of these values four offsets between a quarter and a full beam diameter are selected because the simulation shows that the remelted depth significantly decreases for much larger offsets of the used power ratios of 150W for the first and 50W for the second laser beam. The melting power of the motion synchronized offset strategy equals the melting power of a single reference beam.

For the second experiment a cantilever geometry is used. These components are produced using the most promising settings (shown in table 3), which led to good results in the density experiments and showed promising benefits in the numerical model. Additionally to the offset strategy, the heating strategy is used. For heating strategies a parameter set is necessary in which

the first beam is powerful enough to melt the material by itself and in which the second beam is fast enough to distribute a high amount of power over the cross section.

Table 2: Experimental setting for cubic probe experiments

	Power 1 [W]	Power 2 [W]	Scan Speed [mm/s]	Offset [beam diameter]
Reference	200	0	850	
	200	0	1000	
	200	0	1150	
Offset Strategy	150	50	850	0.25, 0.50, 0,75, 1,00
	150	50	1000	0.25, 0.50, 0,75, 1,00
	150	50	1150	0.25, 0.50, 0,75, 1,00

But the second beam's power should be limited to prevent evaporation of material. Therefore the power of the first laser is set to 200W to be sure that the energy amount is high enough for melting. The second beam's power is set to 50W and can be seen as an additional energy amount for heating. The hatch distance of the heating strategy is varied between 90 μm and 180 μm allowing testing different heating repetition rates for the same scan speeds. The cantilevers are attached to the base plate during the process and cut off afterwards to release the residual stresses and to measure the distortion. The scan speeds of the second laser are chosen based on simulation results.

Table 3: Experimental setting for cantilever experiment

	Power 1 [W]	Power 2 [W]	Scan Speed 1 [mm/s]	Scan Speed 2 [mm/s]	Hatch distance [μm]	Offset [beam diameter]
Reference	200	0	850	0	90	
	200	0	1000	0	90	
Offset strategy	150	50	850	850	90	0.50, 0.75, 1,00
	150	50	1000	1000	90	0.50, 0.75, 1,00
Heating strategy	200	50	1000	3000	180	
	200	50	1000	6000	180	
	200	50	1000	9000	180	
	200	50	1000	3000	90	
	200	50	1000	6000	90	
	200	50	1000	9000	90	

Results & Discussion

Cubic Probes

Figure 6 shows the irradiation of the vaporized material and therefore proofs the functionality of the elaborated offset strategy as it shows the movement and positioning of the laser beams during the process on same melt track. During the build no big change could be

observed so that it can be assumed that the calibration of the scan fields only changed within a small area.
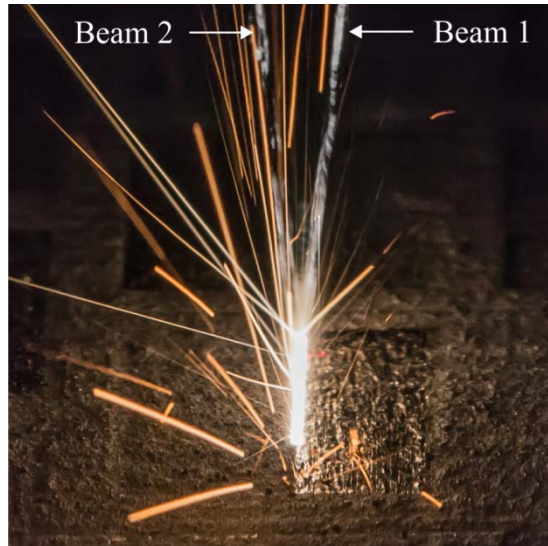

Figure 6: Photograph of the process while manufacturing cubic probes using the offset strategy. The beams are visible due to some irradiation of vaporized material

The results of the density measurements are plotted in figure 7. The values are an average of two repetitions. All three investigated scan speeds show remarkable trends for a rising beam offset in scanning direction. A small offset of just a quarter beam diameter increases the density of the probes while an offset of a half beam diameter decreases it. And offsets of three quarter and a whole beam diameter increase the density even more significantly. Therefore the trend is comparable to the predictions made by the numerical model. The significance of this trend is much higher for the scan speed of 1150 mm/s than for the lower ones. It can be assumed that the microstructures of the 1150 mm/s probes leave more potential for an increase in density due to their higher porosity so that the observed effect is higher as well. All measured densities are about 1% short from what was expected due to prior experiences with single beams. Since the probes were manufactured on a laboratory machine this problem is still under investigation.

As earlier described the driving force of the density increase at higher offsets might be found within the evaporation driven melt pool dynamics. The evaporation forces the melt downwards and to the sides and is therefore supporting the distribution of energy to solidified parts so that these are easier molten. However, using a badly chosen offset might lead to two interfering evaporation spots that prevent each other from forming beneficial down- and sideward melt flows.
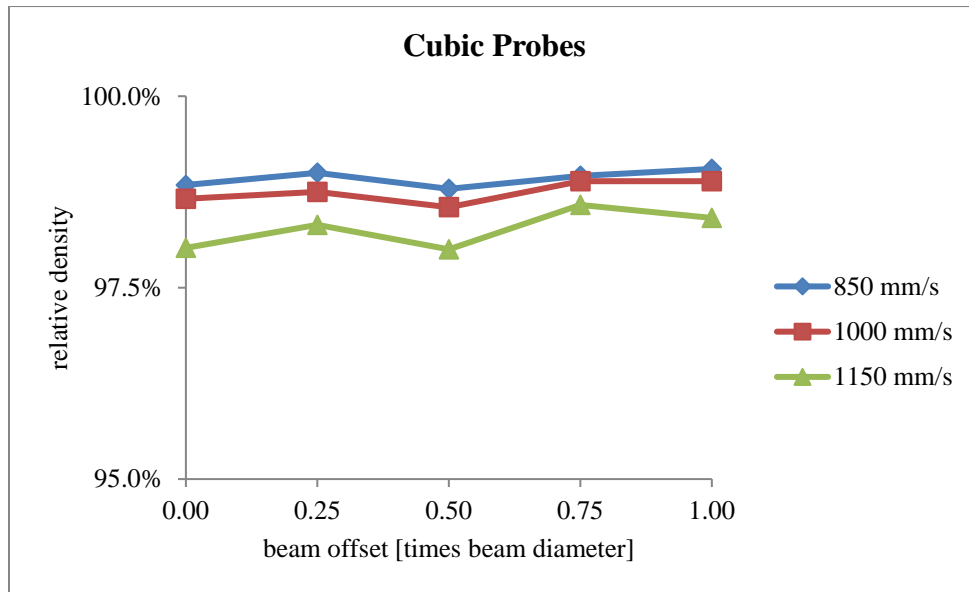
Cubic Probes

Figure 7: Density of cubic probes in relation to the beam offset in scanning direction. The beam offset of 0 is related to the reference probe of a single beam and 200 W. The offset beam powers are 150 W of laser 1 and 50 W of laser 2

Cantilever Probes

The distortion measurement is done using a Leica DCM-3D microscope by focusing the melt tracks of the last layer and therefore measuring the height values of the tracks so that the influence of spatter can be neglected. Three values are taken on the not deformed and three on the deformed side of each cantilever. The measured average results are shown in figure 8. The trends differ for the investigated scan speeds but show the potential to reduce the distortion in all cases. For this first proof of concept the distortion of 850 mm/s is reduced by about 11% using the offset strategy. The distortion of 1000 mm/s is reduced by about 7% using the offset strategy and by about 17% by using the heating strategy. Differences to the trends which were estimated by the numerical tool can be observed since a continuously decrease of distortion was expected for increasing beam offsets. The differences might be explained by the estimation itself in which just an indicator, the temperature gradient based on a single track, was used to estimate the residual stresses after processing.

Furthermore the surface quality of the heating strategy probes needs to be discussed. The surface of the slow heating speeds of 3000 mm/s show a significant worse surface quality than the faster ones. This is due to the reached heating temperatures around the evaporation temperature. Since the heating power is not high enough to reach a sufficient melt pool depth and to connect the melt pool with the previous layer, the evaporation leads to a strong spattering. The effect is reduced with faster scan speeds and a larger hatch and therefore supporting this explanation since the energy is distributed faster and wider so that the risk to evaporate material drops. This observation needs to be considered for using this strategy on real parts because the spattering might increase the porosity due to an inhomogeneous powder distribution as well. Concluding this, a wider spot is necessary to enable a stronger heating with higher powers aiming for a more homogeneous temperature field on a higher temperature level since faster scan speeds are limited by the galvo rotation speeds and the laser on and off delays.
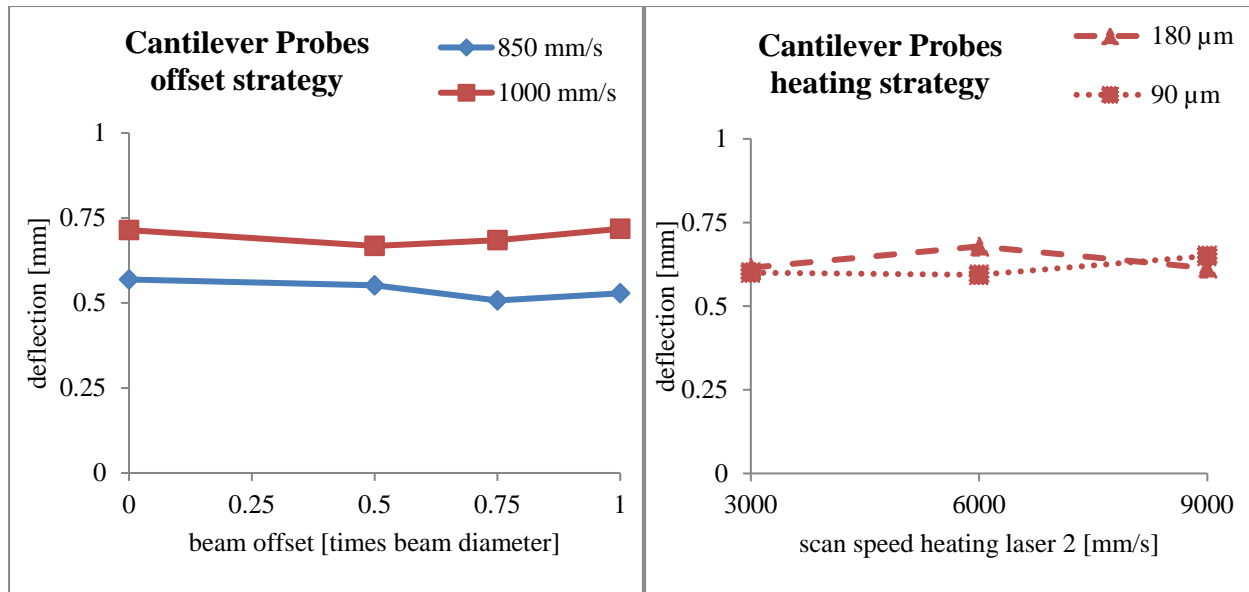
Figure 8: Measured deflection of cantilever structures. Left: Offset strategy using two different speeds and three different offsets as well as two reference probes. Right: Heating strategy testing three different scan speeds of laser 2 at two different hatch distances for a melting beam speed of 1000 mm/s (reference on the left at beam offset 0)

Conclusion & Outlook

The presented simulations and experiments show the potential of multi-beam strategies for the processing of materials in SLM. The investigated offset strategy leads to increasing melt pool dimensions and therefore higher densities at similar speeds and hatch distances and is also able to reduce the residual stresses by reducing the temperature gradients. But the definition of usable beam offsets is of crucial importance because the melt pool dynamics do not favor every beam offset. When using a badly chosen beam offset the density might drop rapidly. Furthermore this strategy is limited due to the necessary calibration procedure and the temperature stability of the machine so that no unintended offset is added during processing.

The heating strategy on the other hand is nearly free of the calibration limitations since the heating beam does not need to be as exact as a second melting beam. But the necessary scan speeds to avoid evaporation by the heating beam are in conflict with the wish to increase the heating powers to homogenize the parts temperature on a higher level. Heating the part solely after melting, will reduce the chance of spattering but might as well fuse spatter to the already solidified layer.

Both strategies need to be studied further on using a wider scope of parameters and materials to evaluate the possibility of these strategies for industrial application. But the shown experiments and simulations offer a proof of concept and promising results for further research. Especially the chance of widening the range of materials because of the in process reduction of stresses seems promising. Additional strategies are possible as well, like e.g. a lateral offset or a vector wise heating strategy and the use of them in combination of them with strategies like the checkerboard scanning.

References

1. Mercelis, P. and Kruth, J.-P., *Residual stresses in selective laser sintering and selective laser melting.* Rapid Prototyping Journal, 2006. 12(5): 254-265
2. Kruth, J.-P., Deckers, J., Yasa, E. and Wauthlé, R., *Assessing and comparing influencing factors of residual stresses in selective laser melting using a novel analysis method.* Proceedings of the Institution of Mechanical Engineers, Part B: Journal of Engineering Manufacture, 2012. 226(6): 980-991
3. Riemer, A., Leuders, S., Thöne, M., Richard, H.A., Tröster, T., Niendorf, T., *On the fatigue crack growth behavior in 316L stainless steel manufactured by selective laser melting.* Engineering Fracture Mechanics, 2014. 120: 15-25
4. Shiomi, M., Osakada, K., Nakamura, K., Yamashita, T. and Abe, F., *Residual Stress within Metallic Model Made by Selective Laser Melting Process.* CIRP Annals – Manufacturing Technology, 2004. 53(1): 195-198
5. Wiesner, A. and Schwarze, D., *Multi-Laser Selective Laser Melting.* 8th International Conference on Photonic Technologies LANE, 2014
6. Trautmann, A., *Bifocal Hybrid Laser Welding: A Technology for Welding of Aluminum and Zinc-coated Steels.* Forschungsberichte IWB, 2009. Vol. 230
7. Zäh, M.F., *Wirtschaftliche Fertigung mit Rapid-Technologien.* Carl Hanser Verlag GmbH & Co. KG, 2006.
8. Böhm, S. and Schulze, K.R., Der Elektronenstrahl als Werkzeug für die Fügetechnik. DVS-Berichte, 2014
9. Schultz, H., *Elektronenstrahlsschweissen. Fachbuchreihe Schweisstechnik.* Verlag für Schweissen und verwandte Verfahren, DVS-Verlag, 2000. Vol. 93
10. Abe, F., Osakada, K., Shiomi, M., Uematsu, K. and Matsumoto, M., *The manufacturing of hard tools from metallic powders by selective laser melting.* Journal of Materials Processing Technology, 2001. 111: 210-213
11. Wilkes, J., Hagedorn, Y.-C., Meiners, W. and Wissenbach, K., *Additive manufacturing of ZrO2-Al2O3 ceramic components by selective laser melting.* Rapid Prototyping Journal, 2011. 19(1): 51-57
12. Son, G., *A level set method for incompressible two-fluid flows with immersed solid boundaries.* Numerical Heat Transfer Part B, 2005. 47: 473-489
13. Son. G. and Hur, N., *A coupled level set and volume-of-fluid method for the buoyancy-driven motion of fluid particles.* Numerical Heat Transfer Part B, 2002. 42: 523-542
14. Gusarov, A.V., Yadroitsev, I., Bertrand, P. and Smurov, M., *Model of Radiation and Heat Transfer in Laser-Powder Interaction Zone at Selective Laser Melting.* Journal of Heat Transfer, 2011. 131: 072101
15. International Atomic Energy Agency, *Thermophysical Properties of Materials for Nuclear Engineering: A Tutorial and Collection of Data*, 2008
16. Ordal, M.A., Bell, R.J., Alexander, R.W., Long, L.L. and Querry M.R., *Optical properties of fourteen metals in the infrared and far infrared – Al, Co, Cu, Au, Fe, Pb, Mo, Ni, Pd, Pt, Ag, Ti, V, and W.* Applied Optics, 1985. 24: 4493-4499 (accessed via refractiveindex.info)